

The Final Measurement of ϵ'/ϵ from KTeV

E. Worcester
 University of Chicago, Chicago, Illinois

We present precise measurements of CP and CPT symmetry based on the full dataset of $K \rightarrow \pi\pi$ decays collected by the KTeV experiment at Fermi National Accelerator Laboratory during 1996, 1997, and 1999. This dataset contains about 15 million $K \rightarrow \pi^0\pi^0$ and 70 million $K \rightarrow \pi^+\pi^-$ decays. We measure the direct CP violation parameter $Re(\epsilon'/\epsilon) = (19.2 \pm 2.1) \times 10^{-4}$. We find the K_L - K_S mass difference $\Delta m = (5265 \pm 10) \times 10^6 \text{ } \hbar\text{s}^{-1}$ and the K_S lifetime $\tau_S = (89.62 \pm 0.05) \times 10^{-12} \text{ s}$. We test CPT symmetry by finding the phase of the indirect CP violation parameter ϵ , $\phi_\epsilon = (44.09 \pm 1.00)^\circ$, and the difference of the relative phases between the CP violating and CP conserving decay amplitudes for $K \rightarrow \pi^+\pi^-$ (ϕ_{+-}) and for $K \rightarrow \pi^0\pi^0$ (ϕ_{00}), $\Delta\phi = (0.29 \pm 0.31)^\circ$. These results are consistent with other experimental results and with CPT symmetry.

1. Introduction

Violation of CP symmetry occurs in the neutral kaon system in two different ways. The dominant effect is the result of an asymmetry in the mixing of K^0 and \bar{K}^0 such that K_L and K_S are not CP eigenstates. This effect is parameterized by ϵ and is called indirect CP violation. The other effect, called direct CP violation, occurs in the $K \rightarrow \pi\pi$ decay process and is parameterized by ϵ' . Direct CP violation affects the decay rates of $K \rightarrow \pi^+\pi^-$ and $K \rightarrow \pi^0\pi^0$ differently, so it is possible to measure the level of direct CP violation by comparing η_{+-} and η_{00} :

$$\begin{aligned}\eta_{+-} &= \frac{A(K_L \rightarrow \pi^+\pi^-)}{A(K_S \rightarrow \pi^+\pi^-)} = \epsilon + \epsilon' \\ \eta_{00} &= \frac{A(K_L \rightarrow \pi^0\pi^0)}{A(K_S \rightarrow \pi^0\pi^0)} = \epsilon - 2\epsilon'\end{aligned}\quad (1)$$

$$Re(\epsilon'/\epsilon) \approx \frac{1}{6} (|\frac{\eta_{+-}}{\eta_{00}}|^2 - 1).$$

Measurements of $\pi\pi$ phase shifts [1] show that, in the absence of CPT violation, the phase of ϵ' is approximately equal to that of ϵ . Therefore, $Re(\epsilon'/\epsilon)$ is a measure of direct CP violation and $Im(\epsilon'/\epsilon)$ is a measure of CPT violation.

For small $|\epsilon'/\epsilon|$, $Im(\epsilon'/\epsilon)$ is related to the phases of η_{+-} and η_{00} by

$$\begin{aligned}\phi_{+-} &\approx \phi_\epsilon + Im(\epsilon'/\epsilon) \\ \phi_{00} &\approx \phi_\epsilon - 2Im(\epsilon'/\epsilon) \\ \Delta\phi &\equiv \phi_{00} - \phi_{+-} \approx -3Im(\epsilon'/\epsilon).\end{aligned}\quad (2)$$

The relation of the complex parameters η_{+-} , η_{00} , ϵ , and ϵ' is illustrated in Fig. 1 using the central values measured by the KTeV experiment.

Experimental results have established that $Re(\epsilon'/\epsilon)$ is non-zero [2, 3, 4, 5]. In 2003, KTeV reported $Re(\epsilon'/\epsilon) = (20.7 \pm 2.8) \times 10^{-4}$ based on data from 1996 and 1997[6]. We now report the final measurement of $Re(\epsilon'/\epsilon)$ from KTeV. The measurement is based on 85 million reconstructed $K \rightarrow \pi\pi$ decays collected in 1996 1997, and 1999. This full sample is two times

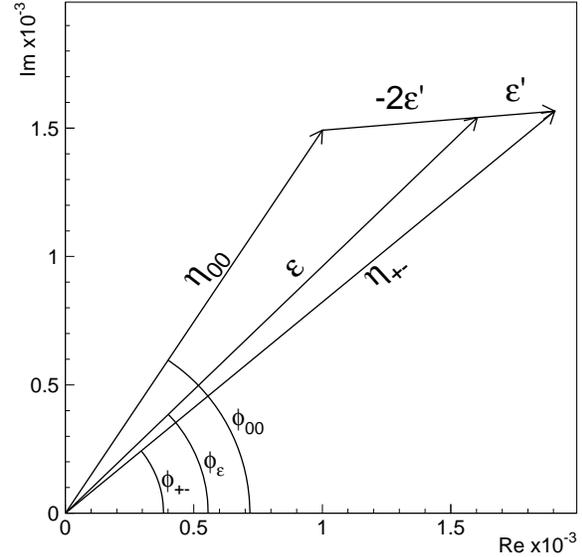


Figure 1: Diagram of CP violating kaon parameters. For this illustration, the parameters have the central values measured by KTeV and the value of ϵ' is scaled by a factor of 50. Although they appear distinct in this diagram, note that ϕ_{+-} and ϕ_{00} are consistent with each other within experimental errors.

larger than, and contains, the sample on which the previous results are based. We also present measurements of the kaon parameters Δm and τ_S , and tests of CPT symmetry based on measurements of $\Delta\phi$ and $\phi_{+-} - \phi_{SW}$.

For these results we have made significant improvements to the data analysis and the Monte Carlo simulation. The full dataset, including those data used in the previous analysis, has been reanalyzed using the improved reconstruction and simulation. These results supersede the previously published results from KTeV. In this presentation, we will focus primarily on improvements to the $K \rightarrow \pi^0\pi^0$ analysis which have reduced the systematic uncertainty in $Re(\epsilon'/\epsilon)$ relative to the previous KTeV result.

2. The KTeV Experiment

The measurement of $Re(\epsilon'/\epsilon)$ requires a source of K_L and K_S decays, and a detector to reconstruct the charged ($\pi^+\pi^-$) and neutral ($\pi^0\pi^0$) final states. The strategy of the KTeV experiment is to produce two identical K_L beams, and then to pass one of the beams through a “regenerator.” The beam that passes through the regenerator is called the regenerator beam, and the other beam is called the vacuum beam. The regenerator creates a coherent $|K_L\rangle + \rho|K_S\rangle$ state, where ρ , the regeneration amplitude, is a physical property of the regenerator. The regenerator is designed such that most of the $K \rightarrow \pi\pi$ decays downstream of the regenerator are from the K_S component. The charged spectrometer is the primary detector for reconstructing $K \rightarrow \pi^+\pi^-$ decays and the pure Cesium Iodide (CsI) calorimeter is used to reconstruct the four photons from $K \rightarrow \pi^0\pi^0$ decays. A Monte Carlo simulation is used to correct for the acceptance difference between $K \rightarrow \pi\pi$ decays in the two beams, which results from the very different K_L and K_S lifetimes. The measured quantities are the vacuum-to-regenerator “single ratios” for $K \rightarrow \pi^+\pi^-$ and $K \rightarrow \pi^0\pi^0$ decay rates. These single ratios are proportional to $|\eta_{+-}/\rho|^2$ and $|\eta_{00}/\rho|^2$, and the ratio of these two quantities gives $Re(\epsilon'/\epsilon)$ via Eq. 1.

2.1. The KTeV Detector

The KTeV detector (Fig. 2) consists of a charged spectrometer to reconstruct $K \rightarrow \pi^+\pi^-$ decays, a pure CsI electromagnetic calorimeter to reconstruct $K \rightarrow \pi^0\pi^0$ decays, a veto system to reduce background, and a three-level trigger to select events. Two virtually identical neutral kaon beams are incident on the detector; a movable active regenerator is placed in one of these beams to provide a coherent mixture of K_L and K_S . In this manner, we collect $K_L \rightarrow \pi\pi$ and $K_S \rightarrow \pi\pi$ decays simultaneously so that many systematic effects cancel in the ratios used to calculate $Re(\epsilon'/\epsilon)$.

The KTeV spectrometer consists of four square drift chambers and a large dipole magnet. Each drift chamber measures charged-particle positions in two planes each in the x and y views. The drift chamber planes have a hexagonal cell geometry formed by six field-shaping wires surrounding one sense wire, and the two planes in each view are offset to resolve position ambiguities. There are a total of 1972 sense wires in the four drift chambers. The magnet imparts a kick of 412 MeV/c in the horizontal plane. The spectrometer measures the momenta of charged particles with an average resolution of 0.4%. The $K \rightarrow \pi^+\pi^-$ reconstruction achieves a z -vertex resolution of 5-30 cm and a mass resolution of 1.5 MeV/ c^2 .

The CsI calorimeter measures the energies and positions of photons from the electromagnetic decay of

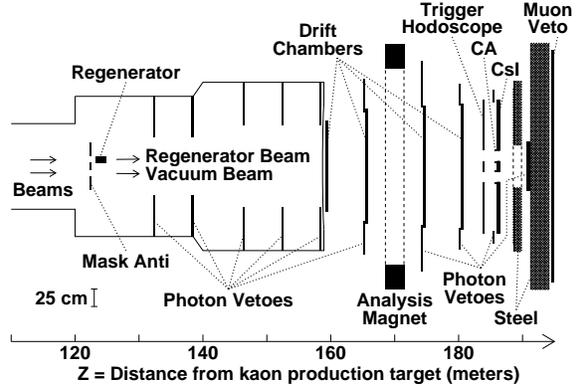


Figure 2: The KTeV Detector

the neutral pions in $K \rightarrow \pi^0\pi^0$ decays. It consists of 3100 pure CsI crystals viewed by photomultiplier tubes. The layout of the 1.9×1.9 m² calorimeter is shown in Fig. 3. There are 2232 2.5×2.5 cm² crystals in the central region, and 868 5×5 cm² crystals surrounding the smaller crystals. The crystals are all 50 cm (27 radiation lengths) long. Momentum analyzed electrons and positrons from $K_L \rightarrow \pi^\pm e^\mp \nu$ decays (K_{e3}) are used to calibrate the CsI energy scale to 0.02%. The CsI calorimeter has an average energy resolution of 0.6%. The reconstructed decay vertex of the neutral pion is directly related to the energies and positions of the photons:

$$Z_{\pi^0} = Z_{CsI} - \frac{r_{12}\sqrt{E_1 E_2}}{m_{\pi^0}}, \quad (3)$$

where r_{12} is the transverse distance between the photons at the CsI and E_1 and E_2 are the photon energies. The $K \rightarrow \pi^0\pi^0$ reconstruction achieves a z -vertex resolution of 20-30 cm and a mass resolution of 1.5 MeV/ c^2 .

KTeV uses an extensive veto system to reject events coming from interactions in the regenerator and to reduce background from kaon decays into non- $\pi\pi$ final states. The veto system consists of a number of lead-scintillator detectors surrounding the decay region and the primary detectors. A three-level trigger, consisting of fast detector signals at Level 1, processing by custom electronics at Level 2, and a software filter at Level 3, is used to select events.

2.2. Monte Carlo Simulation

KTeV uses a Monte Carlo (MC) simulation to calculate the detector acceptance and to model background to the signal modes. The very different K_L and K_S lifetimes lead to very different z -vertex distributions in the vacuum and regenerator beams. We determine the detector acceptance as a function of kaon decay

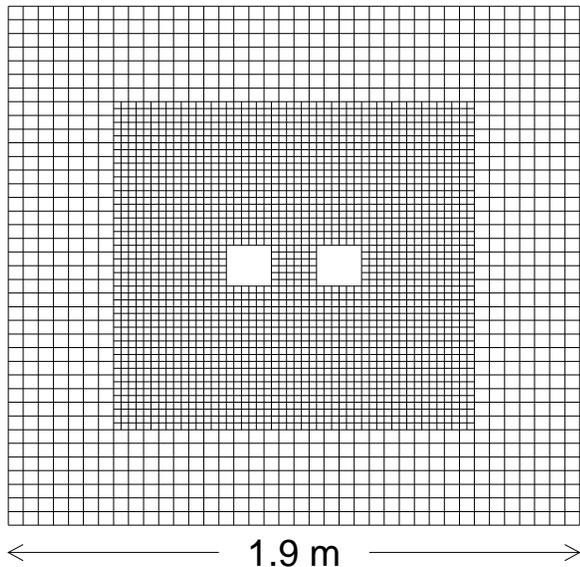


Figure 3: Beamline view of the KTeV CsI calorimeter, showing the 868 larger outer crystals and the 2232 smaller inner crystals. Each beam hole size is $15 \times 15 \text{ cm}^2$ and the two beam hole centers are separated by 0.3 m.

vertex and energy including the effects of geometry, detector response, and resolutions. The simulation of the detector geometry is based both on data and survey measurements. Many aspects of the tracing and detector response are based on libraries created by GEANT[7] simulations. To help verify the accuracy of the MC simulation, we collect and study decay modes with approximately ten times higher statistics than the $K \rightarrow \pi\pi$ signal samples, such as $K_L \rightarrow \pi^\pm e^\mp \nu$ and $K_L \rightarrow \pi^0 \pi^0 \pi^0$.

Many improvements have been made to the MC simulation since the previous result was published in 2003. We have improved the simulation of electromagnetic showers to include the effects of incident particle angles and to simulate the effects of wrapping and shims in the CsI calorimeter. The GEANT library used for the previous analysis was binned in energy and incident position; the effect of angles was approximated by shifting the incident position based on the angle of incidence. The shower library has now been expanded to include nine angles (-35 mrad to 35 mrad) for photons and 15 angles (-85 mrad to 85 mrad) for electrons. Electrons angles may be larger than photon angles because of the momentum kick imparted by the analyzing magnet. Differences between the library angle and the desired angle are approximated by shifting the incident position. The particle energy cutoff applied in the GEANT shower library generation has been lowered from 600 keV to 50 keV for electrons; the photon cutoff of 50 keV is unchanged. Sixteen showers per bin have been generated. Energy deposits are

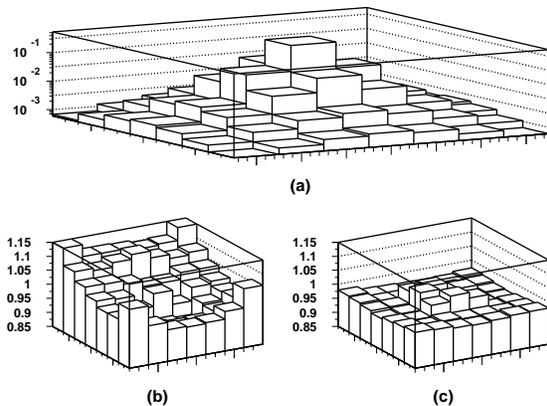


Figure 4: Data-MC comparison of fraction of energy in each of the 49 CsI crystals in an electron shower. (a) The fraction of energy in each of the 49 CsI crystals in an electron shower for data. (b) 2003 data/MC ratio (c) current data/MC ratio

corrected for energy lost in the $12 \mu\text{m}$ mylar wrapping around the CsI crystals and the shims that are present between some rows of CsI crystals.

The current Monte Carlo produces a significantly better simulation of electromagnetic showers in the CsI. Figure 4 shows a data-MC comparison of the fraction of energy in each of the 49 CsI crystals in a shower relative to the total reconstructed shower energy for electrons from $K_L \rightarrow \pi^\pm e^\mp \nu$ decays. The majority of the energy is deposited in the central crystal since the Moliere radius of CsI is 3.8 cm. These particular plots are made for 16-32 GeV electrons with incident angles of 20-30 mrad, but the quality of agreement is similar for other energies and angles. The data-MC disagreement improves from up to 15% for the 2003 MC to less than 5% for the current MC. This improvement in the modeling of electromagnetic shower shapes leads to important reductions in the systematic uncertainties associated with the reconstruction of photon showers from $K \rightarrow \pi^0 \pi^0$ decays.

We have improved the tracing of charged particles through the detector with more complete treatments of ionization energy loss, Bremsstrahlung, delta rays, and hadronic interactions in the drift chambers. The position resolution of the drift chambers was previously treated as flat across the cell; the dependence of the resolution upon position within the cell is now included in the simulation. We have also have updated a number of parameters that go into the kaon propagation and decay calculations.

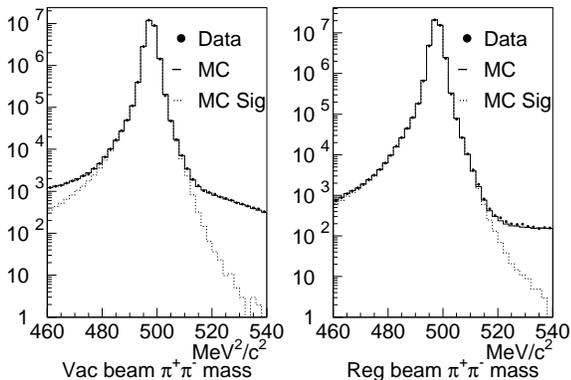


Figure 5: $\pi^+\pi^-$ invariant mass distribution for $K \rightarrow \pi^+\pi^-$ candidate events. The data distribution is shown as dots, the $K \rightarrow \pi^+\pi^-(\gamma)$ signal MC (MC Sig) is shown as a dotted histogram and the sum of signal and background MC is shown as a solid histogram.

3. Data Analysis

The $K \rightarrow \pi^+\pi^-$ analysis consists primarily of the reconstruction of tracks in the spectrometer. The vertices and momenta of the tracks are used to calculate kinematic quantities describing the decay. The $K \rightarrow \pi^+\pi^-$ invariant mass distributions for each beam are shown in Fig. 5.

To reconstruct $K \rightarrow \pi^0\pi^0$ decays, we measure the energies and positions of each cluster of energy in the CsI. A number of corrections are then made to the measured particle energies based on our knowledge of the CsI performance and the reconstruction algorithm. The precision of the CsI energy and position reconstruction is crucial to the $K \rightarrow \pi^0\pi^0$ analysis and has been improved significantly since the previous publication.

We determine the energy deposit in each block of the CsI by converting the digitized information to energies using constants for each channel that are determined from the electron calibration. The laser correction, which is measured using an in-situ laser and corrects for spill-to-spill drifts in each channel's gain, is applied to each block energy. We define "clusters," which are 7×7 arrays of small blocks or 3×3 arrays of large blocks, centered on a "seed block," which contains a local energy maximum. The cluster energy must be corrected for a number of geometric and detector effects. We apply "block-level" corrections, which adjust the energy in each block that makes up the cluster, and "cluster-level" corrections, which are multiplicative corrections to the total cluster energy.

The quality of the calibration and the CsI performance is evaluated by analyzing electrons from the calibration sample with all corrections applied. The electron calibration for 1996, 1997, and 1999 is based on 1.5 billion total electrons. Figure 6 shows the E/p

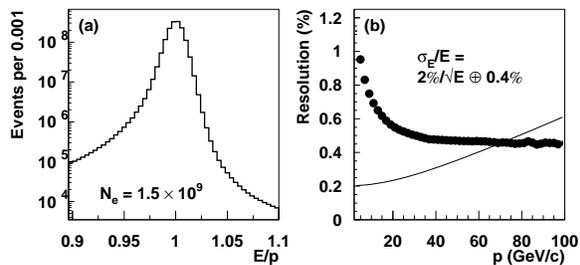


Figure 6: K_{c3} electrons after all corrections. (a) E/p for 1.5×10^9 electrons. (b) Energy resolution. The fine curve shows the momentum resolution function that has been subtracted from the E/p resolution to find the energy resolution.

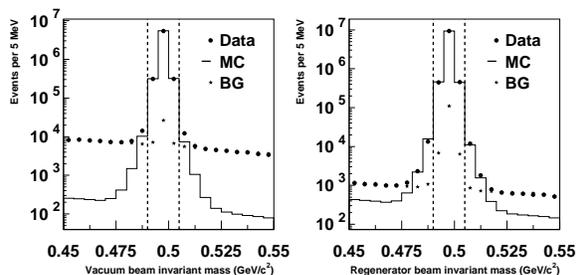


Figure 7: $K \rightarrow \pi^0\pi^0$ $m_{\pi^0\pi^0}$ distributions for for data (dots) and signal MC (histogram) in the vacuum (left) and regenerator (right) beams. The sum of the background MC is also shown (stars). The dashed lines indicate our cuts.

distribution and the energy resolution as a function of momentum after all corrections. The final energy resolution of the calorimeter is $\sigma_E/E \simeq 2\%/\sqrt{E} \oplus 0.4\%$, where E is in GeV.

The position of a cluster is reconstructed by calculating the fraction of energy in neighboring columns and rows of the cluster. The position algorithm uses a map that is based on the uniform photon illumination across each crystal to convert these ratios to a position within the seed block.

We use the cluster energies and positions along with the known pion mass to determine which pair of photons is associated with which neutral pion from the kaon decay and to calculate the decay vertex, the center of energy, and the $\pi^0\pi^0$ invariant mass. The $K \rightarrow \pi^0\pi^0$ invariant mass distributions for each beam are shown in Fig. 7.

For $K \rightarrow \pi^0\pi^0$ decays, the z vertex is determined using only the positions and energies of the four photons in the final state. Therefore, the measured z vertex is dependent upon the absolute energy scale of the CsI calorimeter. The energy scale is set using electrons from $K_L \rightarrow \pi^\pm e^\mp \nu$ decays. A small resid-

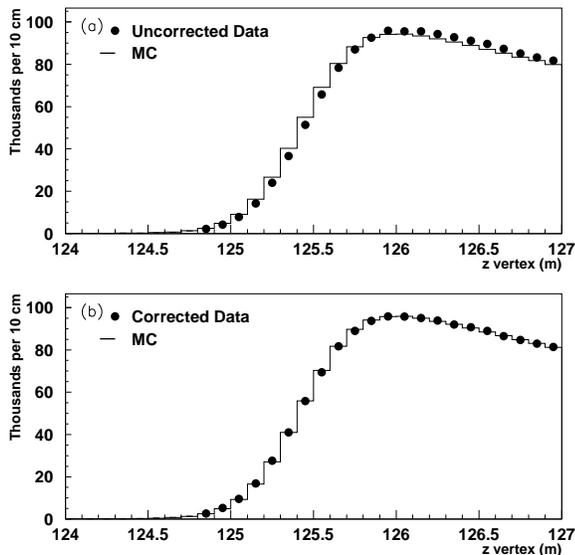


Figure 8: Regenerator beam $K \rightarrow \pi^0 \pi^0$ z -vertex distribution near the regenerator for 1999 data and Monte Carlo. (a) Uncorrected data. (b) Data with energy scale correction applied.

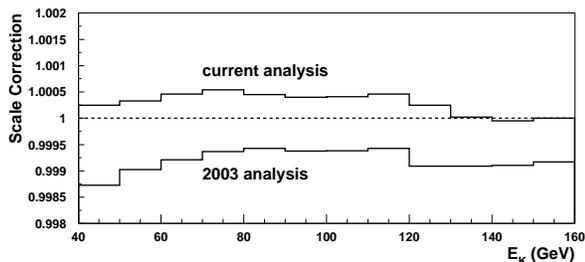


Figure 9: Change in the final energy scale adjustment relative to the 2003 analysis. The dashed line represents no data-MC mismatch.

ual energy scale mismatch between data and Monte Carlo is removed by adjusting the energy scale in data such that the sharp edge in the z -vertex distribution at the regenerator matches between data and Monte Carlo as shown in Fig. 8. The final energy scale adjustment for 1997 data is shown as a function of kaon energy in Fig. 9; the average size of the correction is $\sim 0.04\%$. As a result of improvements to the simulation and reconstruction of clusters, the required energy scale adjustment is smaller and less dependent on kaon energy than in the previous analysis.

Background to the $K \rightarrow \pi\pi$ signal modes is simulated using the Monte Carlo, normalized to data outside the signal region, and subtracted. In this

analysis, we use decays from coherently regenerated kaons only; any kaons that scatter with non-zero angle in the regenerator are treated as background. Scattering background is the same for both $K \rightarrow \pi^+ \pi^-$ and $K \rightarrow \pi^0 \pi^0$ decays so it can be identified using the reconstructed transverse momentum of the decay products in charged mode; we use $K \rightarrow \pi^+ \pi^-$ decays to tune the simulation of scattering background on which we must rely in neutral mode. Non- $\pi\pi$ background is present due to the misidentification of high branching-ratio decay modes such as $K_L \rightarrow \pi^\pm e^\mp \nu$, $K_L \rightarrow \pi^\pm \mu^\mp \nu$, and $K_L \rightarrow \pi^0 \pi^0 \pi^0$. Background contributes less than 0.1% of $K \rightarrow \pi^+ \pi^-$ data and about 1% of $K \rightarrow \pi^0 \pi^0$ data. Tables I and II contain a summary of all the background fractions for each year. There are some variations in background levels among the years due to differences in trigger and veto requirements.

Source	Vacuum Beam		Regenerator Beam	
	1997	1999	1997	1999
Regenerator Scattering	—	—	0.073%	0.075%
Collimator Scattering	0.009%	0.008%	0.009%	0.008%
$K_L \rightarrow \pi^\pm e^\mp \nu$	0.032%	0.032%	0.001%	0.001%
$K_L \rightarrow \pi^\pm \mu^\mp \nu$	0.034%	0.030%	0.001%	0.001%
Total Background	0.074%	0.070%	0.083%	0.085%

Table I Summary of $K \rightarrow \pi^+ \pi^-$ background levels

After all event selection requirements are applied and background is subtracted, we have a total of 25 million vacuum beam $K \rightarrow \pi^+ \pi^-$ decays and 6 million vacuum beam $K \rightarrow \pi^0 \pi^0$ decays. The numbers of events collected in each beam are summarized in Table III.

Table IV summarizes the systematic uncertainties on $Re(\epsilon'/\epsilon)$. We describe the procedure for evaluating several important systematic uncertainties below.

Acceptance: We use the Monte Carlo simulation to estimate the acceptance of the detector in momentum and z -vertex bins in each beam. We evaluate the quality of this simulation by comparing energy-reweighted z -vertex distributions in the vacuum beam between data and Monte Carlo. We fit a line to the data-MC ratio of the z -vertex distributions and call the slope of this line the acceptance “ z -slope.” A z -slope affects the value of $Re(\epsilon'/\epsilon)$ by producing a bias between the regenerator and vacuum beams because of the very different z -vertex distributions in the two beams; we use the known difference of the mean z values for the vacuum and regenerator beams along with the measured z -slope to evaluate the systematic error on $Re(\epsilon'/\epsilon)$.

Figure 10 shows the measured z -slopes for the full $K_L \rightarrow \pi^+ \pi^-$, $K_L \rightarrow \pi^\pm e^\mp \nu$, $K_L \rightarrow \pi^0 \pi^0$, and $K_L \rightarrow \pi^0 \pi^0 \pi^0$ event samples. We use the $\pi^+ \pi^-$ z -

Source	Vacuum Beam			Regenerator Beam		
	1996	1997	1999	1996	1997	1999
Regenerator Scattering	0.288%	0.260%	0.258%	1.107%	1.092%	1.081%
Collimator Scattering	0.102%	0.122%	0.120%	0.081%	0.093%	0.091%
$K_L \rightarrow \pi^0 \pi^0 \pi^0$	0.444%	0.220%	0.301%	0.015%	0.006%	0.012%
Photon Mispairing	0.007%	0.007%	0.008%	0.007%	0.008%	0.007%
Hadronic Production	0.002%	0.001%	—	0.007%	0.007%	0.007%
Total Background	0.835%	0.603%	0.678%	1.209%	1.197%	1.190%

Table II Summary of $K \rightarrow \pi^0 \pi^0$ background levels. Note that photon mispairing is not subtracted from the data and is not included in the total background sum.

	Vacuum Beam	Regenerator Beam
$K \rightarrow \pi^+ \pi^-$	25107242	43674208
$K \rightarrow \pi^0 \pi^0$	5968198	10180175

Table III Summary of event totals after all selection criteria and background subtraction.

Source	Error on $Re(\epsilon'/\epsilon)$ ($\times 10^{-4}$)	
	$K \rightarrow \pi^+ \pi^-$	$K \rightarrow \pi^0 \pi^0$
Trigger	0.23	0.20
CsI cluster reconstruction	—	0.75
Track reconstruction	0.22	—
Selection efficiency	0.23	0.34
Apertures	0.30	0.48
Acceptance	0.57	0.48
Background	0.20	1.07
MC statistics	0.20	0.25
Total	0.81	1.55
Fitting		0.31
Total		1.78

Table IV Summary of systematic uncertainties in $Re(\epsilon'/\epsilon)$.

slope to set the systematic uncertainty and measure the $\pi^\pm e^\mp \nu_e$ z -slope as a crosscheck. For neutral mode, we use the high statistics $\pi^0 \pi^0 \pi^0$ mode to set the systematic uncertainty because it has the same type of particles in the final state as $\pi^0 \pi^0$ and is more sensitive than $\pi^0 \pi^0$ to potential problems in the reconstruction due to close clusters, energy leakage at the CsI edges, and low photon energies.

Energy Scale: The final energy scale adjustment ensures that the energy scale matches between data and MC at the regenerator edge, but we must check whether the data and MC energy scales remain matched for the full length of the decay volume. We check the energy scale at the downstream end of the decay region by studying the z -vertex distribution of $\pi^0 \pi^0$ pairs produced by hadronic interactions in the vacuum window in data and MC. To verify that this

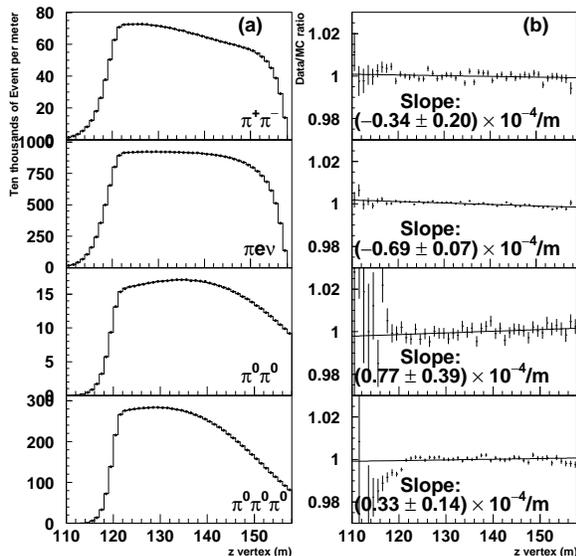


Figure 10: Comparison of the vacuum beam z distributions for data (dots) and MC (histogram). The data-to-MC ratios on the right are fit to a line, and the z -slopes (see text) are shown. All distributions are for the full data sample used in this analysis.

type of production has a comparable energy scale to $K \rightarrow \pi^0 \pi^0$, we also study the z -vertex distribution of hadronic $\pi^0 \pi^0$ pairs produced in the regenerator. The data-MC comparisons of reconstructed z vertex for these samples are shown in Fig. 11.

To convert these shifts to an uncertainty in $Re(\epsilon'/\epsilon)$, we consider a linearly varying energy scale distortion such that no adjustment is made at the regenerator edge and the z shift at the vacuum window is that measured by the hadronic vacuum window sample. The average energy scale distortion we apply is shown by the hatched region in Fig. 11. We rule out energy scale distortions that vary non-linearly as a function of z vertex as they introduce data-MC discrepancies in other distributions. The systematic error on $Re(\epsilon'/\epsilon)$ due to uncertainties in the $K \rightarrow \pi^0 \pi^0$ energy scale is

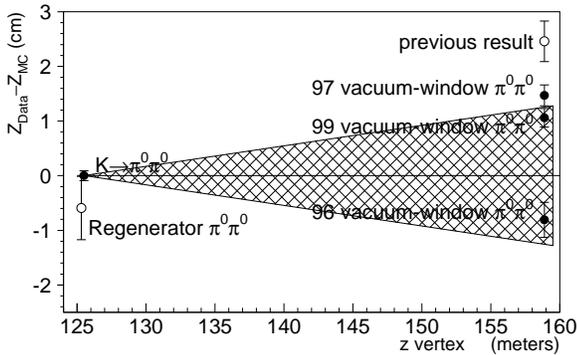


Figure 11: Energy scale tests at the regenerator and vacuum window. The difference between the reconstructed z positions for data and MC is plotted for the $K \rightarrow \pi^0 \pi^0$, regenerator $\pi^0 \pi^0$, and vacuum window $\pi^0 \pi^0$ samples. The solid point at the regenerator edge is the $K \rightarrow \pi^0 \pi^0$ sample; there is no difference between data and MC by construction. The open point at the regenerator edge is the average shift of the regenerator $\pi^0 \pi^0$ samples for all three years. The points at the vacuum window are the shifts for the vacuum window samples for each year separately. The hatched region shows the range of data-MC shifts covered by the total systematic uncertainty from the energy scale. For reference, the data-MC shift at the vacuum window from the 2003 analysis is also plotted.

0.65×10^{-4} ; this is a factor of two smaller than in the previous analysis.

Energy Non-linearity: Some reconstructed quantities in the analysis do not depend on the CsI energy scale, but are sensitive to energy non-linearities. To evaluate the effect of energy non-linearities on the reconstruction, we study the way the reconstructed kaon mass varies with reconstructed kaon energy, kaon z vertex, minimum cluster separation, and incident photon angle. Data-MC comparisons for these distributions for the 1999 data sample are shown in Fig. 12. To measure any bias resulting from the nonlinearities that cause the small data-MC differences seen in these distributions, we investigate adjustments to the cluster energies that improve the agreement between data and MC in the plot of reconstructed kaon mass vs kaon energy. We find that a 0.1%/100 GeV distortion produces the best data-MC agreement for the 1997 and 1999 datasets. Figure 13 shows the improvement in data-MC agreement with this distortion applied to 1999 data. The data-MC agreement in the reconstructed kaon mass as a function of kaon energy has been significantly improved compared to the previous analysis in which a 0.7%/100 GeV distortion was required for 1997 data.

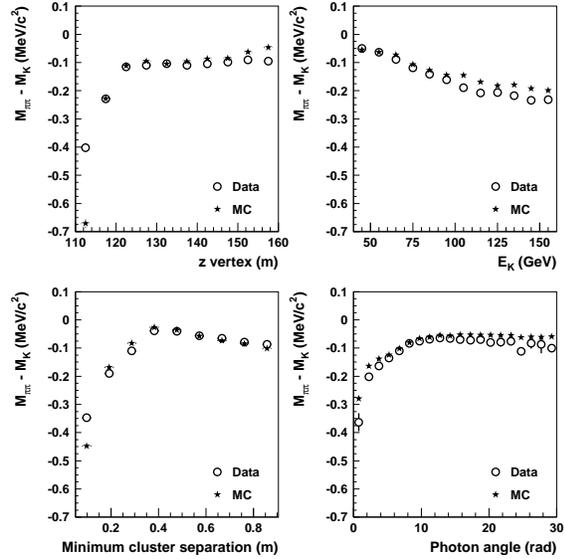


Figure 12: Comparisons of the reconstructed kaon mass vs z -vertex (top left), kaon energy (top right), minimum cluster separation (bottom left), and photon angle (bottom right) for 1999 data and MC. The values plotted are the difference between the reconstructed kaon mass for each bin and the nominal PDG kaon mass.

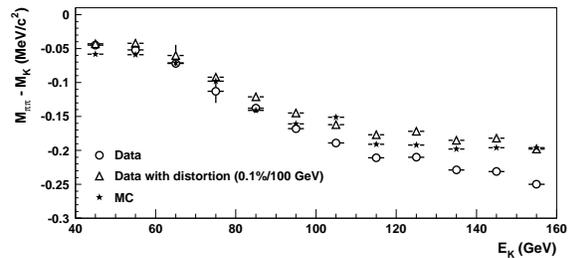


Figure 13: Effect of 0.1%/100 GeV distortion on M_K vs E_K for 1999 data. The values plotted are the difference between the reconstructed kaon mass for each bin and the nominal PDG kaon mass.

4. Results

The value of $Re(\epsilon'/\epsilon)$ and other kaon parameters Δm , τ_S , ϕ_ϵ , and $Im(\epsilon'/\epsilon)$ are determined using a fitting program. The fitting procedure is to minimize χ^2 between background subtracted data yield and a prediction function. The prediction function uses the detector acceptance determined by the Monte Carlo simulation. The fits are performed in 10 GeV/ c kaon momentum bins. To determine $Re(\epsilon'/\epsilon)$, we use the z integrated data yield; to measure the other kaon parameters a z -binned fit is performed.

In the fit for $Re(\epsilon'/\epsilon)$, the inputs are the observed

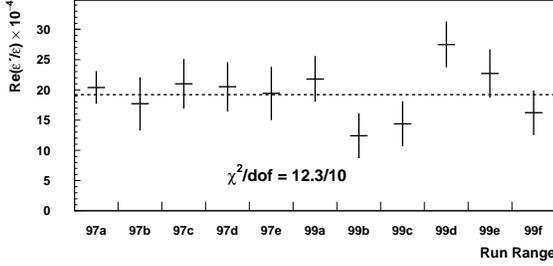


Figure 14: $Re(\epsilon'/\epsilon)$ in subsets of the data sample. Each point is statistically independent. The dashed line indicates the value of $Re(\epsilon'/\epsilon)$ for the full data sample. The 97a run range includes the 1996 $K \rightarrow \pi^0 \pi^0$ data.

number of $K \rightarrow \pi^+ \pi^-$ and $K \rightarrow \pi^0 \pi^0$ decays in each of twelve 10 GeV/c momentum bins. The kaon fluxes for $K \rightarrow \pi^+ \pi^-$ and $K \rightarrow \pi^0 \pi^0$ in each momentum bin, the regeneration parameters, and $Re(\epsilon'/\epsilon)$ are free parameters. CPT symmetry is assumed by setting the phases ϕ_{+-} and ϕ_{00} equal to the superweak phase. The final KTeV measurement of $Re(\epsilon'/\epsilon)$ for the full 1996, 1997, and 1999 combined dataset is:

$$\begin{aligned} Re(\epsilon'/\epsilon) &= [19.2 \pm 1.1(stat) \pm 1.8(syst)] \times 10^{-4} \\ &= [19.2 \pm 2.1] \times 10^{-4}. \end{aligned} \quad (4)$$

The fit quality, quantified by $\chi^2/\nu = 22.9/21$, is good.

We perform several checks of our result by breaking the data into subsets and checking the consistency of the $Re(\epsilon'/\epsilon)$ result. To check for any time dependence, we break the data into 11 run ranges with roughly equal statistics. We divide the data based on beam intensity, regenerator position, magnet polarity, and direction in which the tracks bend in the magnet. We check for dependence of the result on kaon momentum by breaking the data into twelve 10 GeV/c momentum bins. The $Re(\epsilon'/\epsilon)$ results for these tests are shown in Figs. 14, 15, and 16. We find consistent results in all of these subsamples.

The combined result for 1996 and 1997 data only is $Re(\epsilon'/\epsilon) = [20.0 \pm 1.7(stat)] \times 10^{-4}$. This result is consistent with the previously published KTeV result, which is based on the same subset of data, of $Re(\epsilon'/\epsilon) = [20.7 \pm 1.5(stat)] \times 10^{-4}$ [6].

The value of $Re(\epsilon'/\epsilon)$ is consistent with other experimental results. The weighted average of the new KTeV result with previous measurements is $Re(\epsilon'/\epsilon) = [16.8 \pm 1.4] \times 10^{-4}$; see Fig. 17. The consistency probability of these results is 13%.

The regenerator beam decay distribution is sensitive to the kaon parameters τ_S , Δm , ϕ_ϵ , $Re(\epsilon'/\epsilon)$, and $Im(\epsilon'/\epsilon)$. We measure these parameters by fitting the decay vertex distribution in the regenerator beam using a single, z-binned fit. The five kaon parameters, τ_S , Δm , ϕ_ϵ , $Re(\epsilon'/\epsilon)$, and $Im(\epsilon'/\epsilon)$ are free parameters of the z-binned fit. The fit thus provides the most

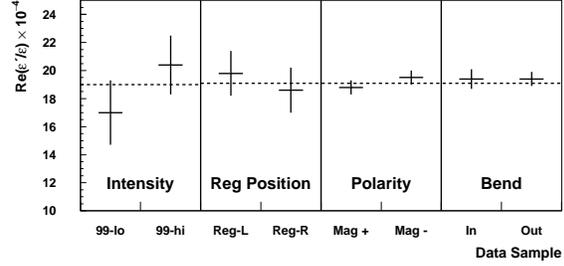


Figure 15: $Re(\epsilon'/\epsilon)$ consistency with beam intensity, regenerator position, magnet polarity, and track bend. The low and high intensity samples are from 1999 only and have average rates of $\sim 1 \times 10^{11}$ protons/s and $\sim 1.6 \times 10^{11}$ protons/s, respectively. Reg-left and reg-right refer to the position of the regenerator beam in the detector. Mag+ and Mag- are the magnet polarity and in/out are the bend of the tracks in the magnet. In the polarity and bend subsets the $K \rightarrow \pi^0 \pi^0$ sample is common to both fits; the errors are estimated by taking the quadrature difference with the error for the full dataset. The dashed lines indicate the value of $Re(\epsilon'/\epsilon)$ in the appropriate full data sample.

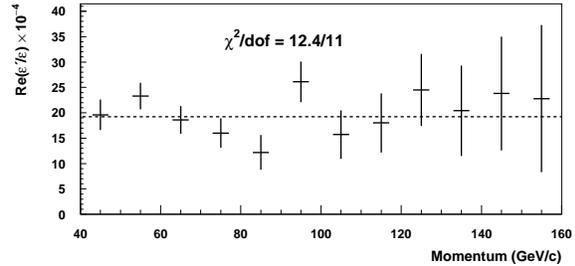


Figure 16: $Re(\epsilon'/\epsilon)$ in 10 GeV/c momentum bins. The dashed line indicates the value for the full data sample.

general description of the data with no requirement of CPT invariance. All the systematic uncertainties are evaluated for the fit using a procedure identical to that used for the $Re(\epsilon'/\epsilon)$ measurement, and accounting for correlations between the parameters. CPT invariance is imposed *a posteriori*, including the total errors of the parameters with their correlations, to obtain a precise measurement of Δm and τ_S .

This approach allows a self-consistent analysis of the data with and without CPT constraints. The results are crosschecked with separate fits for Δm and τ_S performed with CPT invariance imposed *a priori*. The two procedures agree to within $1.3\sigma_{stat}$ and the total uncertainties agree to within $\sim 10\%$.

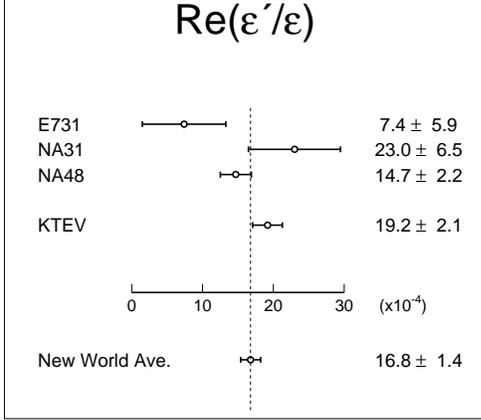


Figure 17: New world average for $Re(\epsilon'/\epsilon)$ combining results from E731[2], NA31[3], NA48[5], and KTeV.

The results of the single z-binned fit are:

$$\begin{aligned}
 \Delta m|_{\text{cpt}} &= [5269.9 \pm 12.3] \times 10^{-12} \text{ s}, \\
 \tau_S|_{\text{cpt}} &= [89.623 \pm 0.047] \times 10^6 \text{ h/s}, \\
 \phi_{+-} &= [43.76 \pm 0.64]^\circ, \\
 \phi_{00} &= [44.06 \pm 0.68]^\circ, \\
 \delta\phi &= \phi_\epsilon - \phi_{SW} = [0.40 \pm 0.56]^\circ, \\
 \Delta\phi &= -3\text{Im}(\epsilon'/\epsilon) = [0.30 \pm 0.35]^\circ.
 \end{aligned} \tag{5}$$

The fit quality is good: $\chi^2/\nu = 425.4/(432 - 33)$. The correlations among these results are shown in Fig. 18 and Fig. 19. The value of $\delta\phi = \phi_\epsilon - \phi_{SW}$ is consistent with zero as expected from CPT invariance in $K^0 - \bar{K}^0$ mixing and the value of $\Delta\phi$ is consistent with zero as expected from CPT invariance in a decay amplitude.

5. Conclusion

Using the full data sample of the KTeV experiment, we have made improved measurements of direct CP violation and other parameters of the neutral kaon system. All of these results supersede previous KTeV results.

Assuming CPT invariance, we measure the direct CP violation parameter

$$\begin{aligned}
 Re(\epsilon'/\epsilon) &= [19.2 \pm 1.1(\text{stat}) \pm 1.8(\text{syst})] \times 10^{-4} \text{ (6)} \\
 &= [19.2 \pm 2.1] \times 10^{-4}.
 \end{aligned}$$

Also under the assumption of CPT invariance, we report new measurements of the $K_L - K_S$ mass difference and the K_S lifetime:

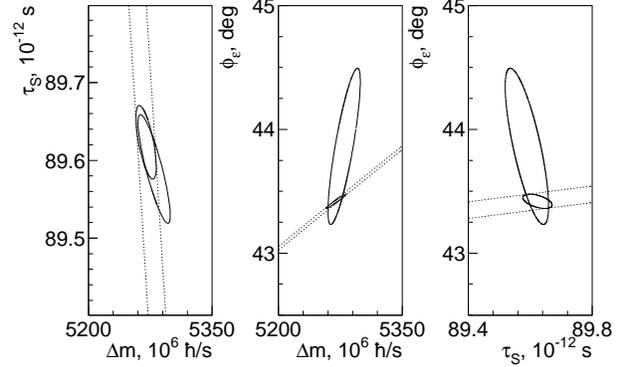


Figure 18: $\Delta\chi^2 = 1$ contours of total uncertainty for (a) $\Delta m - \tau_S$, (b) $\phi_\epsilon - \Delta m$ and (c) $\tau_S - \phi_\epsilon$. Larger ellipses correspond to the z-binned fit without CPT invariance assumption. Dashed lines correspond to $\phi_\epsilon = \phi_{SW}$ CPT constraint. Smaller ellipses are obtained after applying this constraint.

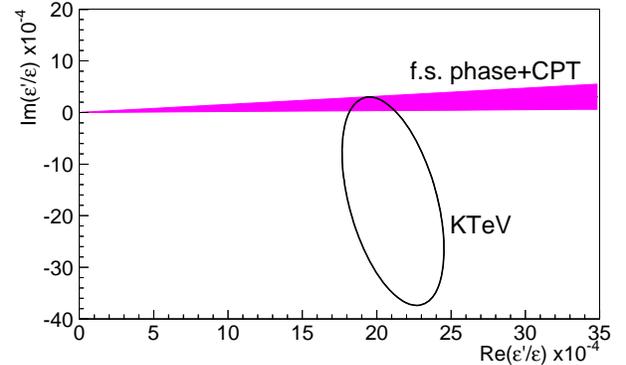


Figure 19: $\Delta\chi^2 = 1$ contour for $Re(\epsilon'/\epsilon)$ vs $Im(\epsilon'/\epsilon)$ as measured by KTeV compared to the measurement of $\pi\pi$ phase shifts [1] and the CPT invariance expectation.

$$\begin{aligned}
 \Delta m &= [5269.9 \pm 12.3] \times 10^{-12} \text{ s} \\
 \tau_S &= [89.623 \pm 0.047] \times 10^6 \text{ h/s}.
 \end{aligned} \tag{7}$$

To test CPT symmetry, we measure the phase differences

$$\begin{aligned}
 \Delta\phi &= -3\text{Im}(\epsilon'/\epsilon) \\
 &= [0.30 \pm 0.35]^\circ,
 \end{aligned} \tag{8}$$

and

$$\phi_\epsilon - \phi_{SW} = [0.40 \pm 0.56]^\circ. \tag{9}$$

These phase results are consistent with CPT invariance in both the decay amplitudes and $K^0 - \bar{K}^0$ mixing.

After decades of experimental effort, direct CP violation in the neutral kaon system has now been measured with an uncertainty of about 10%. Considerable

improvement in theoretical calculations of $Re(\epsilon'/\epsilon)$ will be required to take advantage of this experimental precision. There is some optimism, however, that the next rounds of calculations using lattice gauge theory may approach a 10% uncertainty, making the precise measurements of ϵ'/ϵ equally precise tests of the Standard Model.

Acknowledgments

We gratefully acknowledge the support and effort of the Fermilab staff and the technical staffs of the participating institutions. This work was supported in part by the U.S. Department of Energy, The National Science Foundation, and the Ministry of Education and Science in Japan.

References

- [1] W. Ochs, *πN Newsletter* 3, 25 (1991).
- [2] L.K. Gibbons et al. (E731), *Phys. Rev. Lett.* 70, 1203 (1993).
- [3] G.D. Barr et al. (NA31), *Phys. Lett.* B317, 223 (1993).
- [4] A. Alavi-Harati et al. (KTeV), *Phys. Rev. Lett.* 83, 22 (1999).
- [5] A. Lai et al. (NA48), *Eur Phys. J. C* 22, 231 (2001).
- [6] A. Alavi-Harati et al. (KTeV), *Phys. Rev.* D67, 012005 (2003).
- [7] R. Brun et al., *GEANT* 3.21, CERN, Geneva (1994).